ARTICLE IN PRESS

Available online at www.sciencedirect.com

ScienceDirect

Advances in Space Research xxx (2014) xxx–xxx

ADVANCES IN SPACE RESEARCH (a COSPAR publication)

www.elsevier.com/locate/asr

Free fall tests of the accelerometers of the MICROSCOPE mission

F. Liorzou [a,*], D. Boulanger [a], M. Rodrigues [a], P. Touboul [a], H. Selig [b]

[a] ONERA – The French Aerospace Lab, 29 avenue de la Division Leclerc, F-92322 Châtillon, France
[b] ZARM, University of Bremen, 28359 Bremen, Germany

Received 20 June 2013; received in revised form 3 April 2014; accepted 12 May 2014

Abstract

The MICROSCOPE mission is fully dedicated to the in-orbit test of the Universality of free fall, the so-called Weak Equivalence Principle (WEP), with an expected accuracy better than 10^{-15}. The test principle consists in comparing the accelerations of two proof masses of different composition in the Earth gravitational field. The payload embarks two pairs of test-masses made of Platinum Rhodium and Titanium alloys at the core of two dedicated coaxial electrostatic accelerometers. These instruments are under qualification for a launch in 2016.

Their operations are only possible in microgravity environment which makes its validation on ground a real issue. In Europe, only the drop tower of the ZARM Institute provides a facility for experiments under conditions of weightlessness and offers the experimental conditions to verify the correct functioning of the MICROSCOPE payload. The height of the tower limits the "free fall" experiment period to 4.72 s. Under this strong constraint, the demonstration of the capability to control the test masses of the two coaxial electrostatic accelerometers is challenging. This paper describes the complete experimental set up and in which condition the test has been performed, then an analysis of a drop result is given with its interpretations.

Keywords: Electrostatic accelerometer; Free fall test; Equivalence principle

1. Introduction

The MICROSCOPE mission is fully dedicated to the in-orbit test of the Universality of free fall, the so-called Weak Equivalence Principle (WEP), with an expected accuracy better than 10^{-15} (Touboul et al., 2012a; Hudson et al., 2007). The test principle consists in comparing the accelerations of two proof masses of different composition in the Earth gravitational field. To achieve this goal, the payload of the MICROSCOPE satellite is a double electrostatic accelerometer composed of two cylindrical and concentric test masses made of different material (Platinum Rhodium and Titanium alloys). The instrument measures the difference of accelerations needed to be applied on two test-bodies to keep identical position vs. their reference while submitted to the same gravity. A non-null difference indicates a violation of the WEP.

Based on GOCE legacy, the MICROSCOPE payload developments re-use some very well-known and mastered processes and technologies concerning the electronics, as well as the accelerometer mechanical cores. One of the main differences, performance apart, relies on the ground tests and the validation of the instrument. In the previous developments for the GRACE and GOCE missions (Touboul et al., 2012b), the accelerometers provide the possibility of extensive functional tests on ground by levitating the proof mass under gravity. It was then possible to finely tune the servo-loops of the horizontal axes (normal to the

* Corresponding author. Tel.: +33 1 46 73 48 52; fax: +33 1 46 73 48 24.
E-mail addresses: francoise.liorzou@onera.fr (F. Liorzou), damien.boulanger@onera.fr (D. Boulanger), manuel.rodrigues@onera.fr (M. Rodrigues), pierre.touboul@onera.fr (P. Touboul), selig@zarm.uni-bremen.de (H. Selig).

http://dx.doi.org/10.1016/j.asr.2014.05.009
0273-1177/

1 g direction), while operating in their flight condition. In the case of the MICROSCOPE mission, the satellite will embark accelerometers with heavy test-masses (up to 1.4 kg) and large distances between the masses and the electrodes: 600 μm instead of 300 μm for GOCE. This instrumental configuration, due to the performance requirement, does not let any opportunity to envisage a 1 g suspension. Then, the fine tuning of the servo loop correctors has to be done under microgravity environment.

In Europe the only facility for such tests is the ZARM 120-meter high free fall tower in Bremen, which offers 4.7 s of free fall in vacuum (Christian Eigenbrod, 2007). The main difficulty is to ensure an optimised drop condition in terms of environment disturbances and to achieve the proof mass acquisition and control within the short drop duration. After a general presentation of the MICROSCOPE instrument, the free fall test itself is described. Then, the scientific return from the free falls is highlighted and quantified.

2. The MICROSCOPE instrument

The MICROSCOPE satellite payload is composed of two double accelerometers, each including two cylindrical and concentric test masses. The masses are made of the same material for the first one which is dedicated to assess the accuracy of the WEP experimentation and the level of systematic disturbing errors. The test mass materials are different for the second one (Fig. 1).

Then, the experimentation procedure, in space, is based on a double comparison in order to suppress the systematic errors (Guiu et al., 2007). The selection of the mass material is a compromise between the instrument accuracy requirements, the theoretical interest and the technology feasibility.

Each of the two independent SAGE (Space Accelerometers for gravity Experiment) instruments includes two cylindrical and co-axial masses, each of them surrounded by cylindrical electrode parts (see Fig. 2). The two test masses have identical moment of inertia along their three axes in order to minimize the gravity gradient effect (the requirement in the relative accuracy of the moments of inertia matrix is indeed from 2 to 5.3×10^{-6} (Touboul, 2009).

The electrode parts are in gold plated silica in order to ensure the thermal stability. The sensor unit core is maintained in vacuum with a pressure lower than 10^{-5} Pa thanks to an Invar tight housing and a getter material on top of the sensor unit. The only physical contact with the levitated proof mass is a 7 μm diameter gold wire. The purpose of this wire is to applied an electrical potential to the mass. This potential is composed of a constant part used to linearize the electrostatic actuation force (by biasing the configuration with a DC V_p electric potential applied on the mass, the pressures are no more symmetric and the resultant force is proportional to V_p when the geometrical configuration is perfectly symmetric) and a 100 kHz sinusoid part used to detect the position of the proof mass. Control loops maintain the mass centred and motionless. The same electrodes are used for the measurement of the position of the mass through variation of capacitances and they are also used for the electrostatic control of the six degrees of freedom of the mass.

The mechanical heart of the sensor is connected to the front end electronic unit (FEEU) linked to the interface control unit (ICU). The first unit handles the low-noise analog functions: capacitive sensing of both masses, generation of the reference voltage sources and amplification of the servo-control voltages for the electrostatic actuation. The second unit hosts the digital electronics for the proof-masses servo-loops and the interfaces to the data

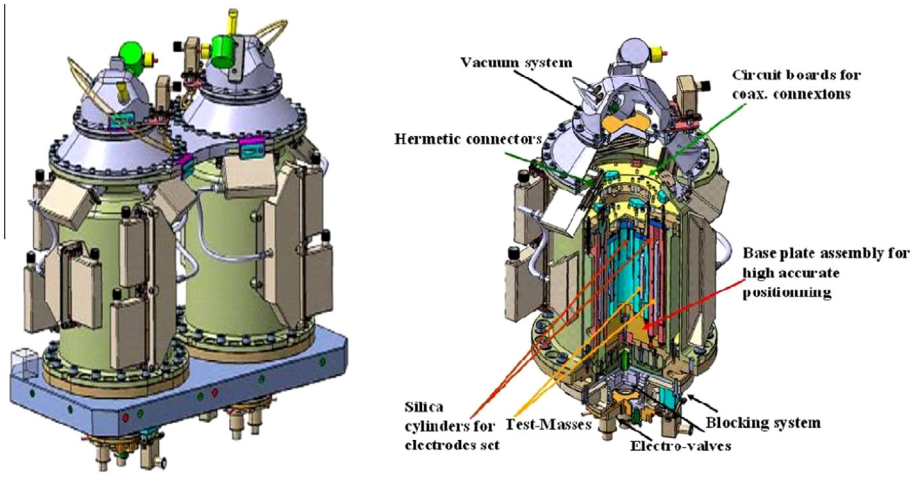

Fig. 1. *Right* – cross cut view of the double accelerometer sensor unit, consisting of two concentric sensors, each including one test-mass and two electrode cylinders, both are in a tight housing with below the blocking mechanism and above the vacuum system, *Left* – sketch of the two accelerometers, REFerence (internal test mass 407.2 g in platinum, external test mass 1387.1 g in platinum) and EP (internal test mass 407.2 g in platinum, external test mass 306.5 g in titanium), when integrated in the satellite (accelerometer EP not tested in the Bremen drop tower).

Please cite this article in press as: Liorzou, F., et al. Free fall tests of the accelerometers of the MICROSCOPE mission. J. Adv. Space Res. (2014), http://dx.doi.org/10.1016/j.asr.2014.05.009

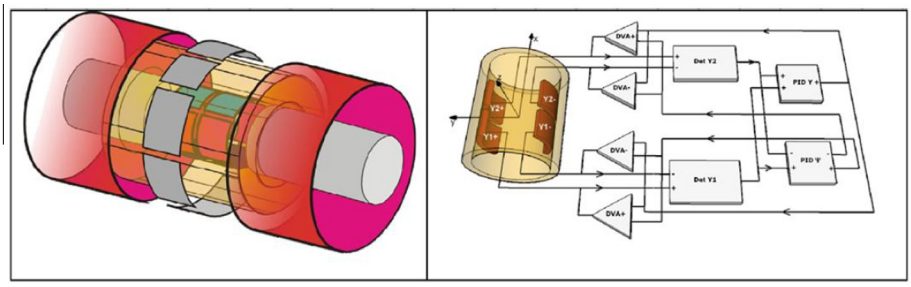

Fig. 2. *Left* – electrode configuration of one sensor unit: the mass (*in yellow*) includes an inner silica cylinder carrying four pairs of quadrant electrodes (*in blue* and *red*) devoted to the radial test-mass control; the outer gold coated cylinder supports two cylindrical electrodes (*in pink*) at the ends of the mass and four pairs of electrodes at the centre (*in green*) in regard to the flat areas for the axial control. *Right* – sketch of the two servo-loops associated to the two pairs of electrodes for the control of *Yi* and the rotation about *Zi*. (For interpretation of the references to colour in this figure legend, the reader is referred to the web version of this article.)

bus of the satellite. The ICU includes also the power converters.

The operation of the accelerometer is similar along the six degree of freedom. It is detailed hereafter along the main measurement axis which is the cylinder axis (*X* axis): when the mass moves along this axis, opposite variations of the recovering surfaces between the proof mass and the electrodes appear leading to a difference of capacitances between the mass and each electrode corresponding to an analog signal provided by the position detector. This signal is digitised and processed by the control loop laws in order to generate a voltage proportional to the sensor acceleration. This voltage is amplified and applied to the electrodes in order to keep the mass at the centre of the two electrodes through electrostatic forces. The selected control law for each mass (each degree of freedom) has a PID (Proportional, Integral, Derivative) configuration. The optimisation of these controllers taking into account the test conditions are made possible by the use of parameters patchable inside the digital electronics of the ICU.

3. Free fall test

The test presented in this paper is performed with the MICROSCOPE qualification model in which the two proof masses of the accelerometers are made of Pt–Rh alloy. Due to the very short free-fall duration and the small range of the accelerometer, the electronics configuration has been modified with respect to the flight configuration. During the free fall test, the electronic power supply is boosted to 90 V instead of the nominal flight supply of 48 V in order to increase the applied voltage capabilities and thus the electrostatic forces for the proof mass acquisition. The DC voltage applied to the mass is also changed from 40 to 80 V which increases the passive electrostatic stiffness between the proof mass and the electrode structure to focus on stability.

Table 1 provides the maximum acceleration that can be applied by the dedicated electronics during the drop tower test; the values for the flight are given in parenthesis. The maximum displacement to be controlled and nullified by each servo-loop is also provided for each degree of freedom as well as *T*min: *T*min is the necessary duration to move the mass from its maximum off-centring to the centre of the core with the maximum acceleration that can be delivered by the electrostatic actuators; *T*min is representative of the difficulty to obtain the full electrostatic levitation of the mass during the duration of the fall.

3.1. Test set up and condition

3.1.1. Capsule integration

The accelerometer and its electronics are accommodated in a cylindrical capsule (2 m high and 80 cm in diameter). Its weight is about 300 kg with its electronics, its on-board data acquisition computer and the experiment payload. At the bottom of the capsule, a 50 cm long cone stabilises it during the deceleration inside the 8 m high braking tank filled with fine graded polystyrol. The deceleration process lasts about 0.2 s and the maximum deceleration rate does not exceed 400 m/s^2 (40 g) and can be applied without damage to the instrument.

The orientation of the sensors is chosen as described in the Fig. 3, *Y* axis in the direction of the fall.

The residual drag of the capsule will be then measured along the *Y* axis of the sensor. The accelerometers are integrated with their *X* axis normal to the axis of symmetry of the capsule, and their *Y* axis aligned with. Optimisation of the capsule balance is a key point in the experiment preparation: without any prior balancing of the capsule, the centre of gravity is no more located on the capsule axis of symmetry, aligned with the two sensor units *Y* axis. Prior to the fall, the capsule is attached at the centre of its top and thus the capsule axis of symmetry is no more vertical because misaligned with the direction between the point of attachment and the centre of gravity. Consequently, when falling, part of the residual atmospheric drag is projected from the fall vertical axis to the *X* and *Z* axes of the accelerometers which are not in the horizontal plan.

3.1.2. Control loop implemented for the fall: simulation

For the free fall tests, the electronic parameters are optimised with a Simulink Matlab simulation tool. Based on the equation of the core physics and on the proposed

Please cite this article in press as: Liorzou, F., et al. Free fall tests of the accelerometers of the MICROSCOPE mission. J. Adv. Space Res. (2014), http://dx.doi.org/10.1016/j.asr.2014.05.009

Table 1

Degrees of freedom	Controlled ranges, in absolute values [m s^{-2}] or [rad s^{-2}]		Maximum displacement to be controlled ©	Tmin (d)
	Internal mass drop (flight)	External mass drop (flight)	Internal and external masses	Internal/external masses
X	7.3×10^{-5} (1.8×10^{-6})	3.8×10^{-5} (9.5×10^{-7})	150 μm	2.02 s/2.8 s
Y	3.3×10^{-4} (4.3×10^{-6})	4.3×10^{-4} (5.6×10^{-6})	150 μm	0.95 s/0.83 s
Z	3.3×10^{-4} (4.3×10^{-6})	4.3×10^{-4} (5.6×10^{-6})	150 μm	0.95 s/0.83 s
Θ	6.4×10^{-3} (6.3×10^{-5})	4.6×10^{-3} (4.5×10^{-5})	7 mrd	1.48 s/1.74 s
Ψ	6.4×10^{-3} (6.3×10^{-5})	4.6×10^{-3} (4.5×10^{-5})	7 mrd	1.48 s/1.74 s
Φ	1.1×10^{-3} (6.3×10^{-5})	6.9×10^{-4} (3.4×10^{-5})	8.6 mrd	3.95 s/4.99 s

control laws for the flight configuration, the parameters of the controllers are derived taking into account the specificity of the test environment and the duration constraints.

The Simulink simulation consists of a block diagram representing the test-mass kinematics inside the sensor core and each function of the control loop electronics. The proof mass motion is modelled by six double integration of the mass accelerations: three positions and three attitudes (weak variations of angle). These accelerations equal the computed applied forces by the generated electrical field. This block also includes rebound conditions when the mass hits the stops during the transient phase of the mass levitation. For each degree of freedom, the mass position is then measured by the capacitive sensor simulated by a block which provides the conversion from position to voltage taking into account the sensor transfer function. The output of this block is limited to 10 V, representative of the electronic circuit saturation.

The PID block contains parallel implementation of the proportional, derivative and integrate transfer functions, followed by another saturation limit. The parameters of the correctors have been determined in order to obtain the desired bandwidth, sufficient gain and phase margins for satisfactory loop stability while integrating the free fall test constraints: the limited time duration and the environmental disturbances due to the capsule release.

Indeed, because of the duration of the falls, the system must be faster to desaturate than in orbit. The integral action of the corrector, while allowing the removal of fine static residual errors, saturates the transient response of the loop and does not add any interest in the limited 4.7 s of the fall. It has been removed in the presented free-fall configuration. Concerning the environmental disturbances, the model includes the aerodynamic drag of the capsule, proportional to the square of the capsule velocity. At the end of the fall, it reaches 10 μg (with a residual pressure in the tube of 10 Pa).

The block diagram of the simulation is presented in Fig. 4. On this figure, the electrostatic actuator includes the electronic amplifiers (gain, bandwidth, saturation) which generate on the set of electrodes around the mass the needed charges and the expression of the corresponding electrostatic forces applied to the mass.

The close loop transfer function, using s as the frequency variable, can be expressed as:

$$a_{\text{app}}/a_{\text{ext}} = \mathrm{H}(s)/(s^2 + \omega_s^2 + \mathrm{H}(s)) \sim \omega_c^2/(s^2 + \omega_c^2) \quad (1)$$

With H(s), the transfer function of the loop simplified in:

$$\mathrm{H}(s) = \omega_c^2(1 + \mathrm{bs} + c/s) \quad (2)$$

b and c provides respectively the stability and the accuracy of the loop, ω_s is the angular frequency corresponding to the electrostatic stiffness and ω_c the natural angular frequency of the loop.

ω_c^2 is, for example, equal to 25.84 (rad/s)^2 on Y axis external mass.

For the simulation, a Monte-Carlo distribution of the initial conditions of the drop, proof mass position and velocity, is applied in order to figure out the temporal trend response of the instrument during the fall. The simulations demonstrate that the servo-loop convergence is achieved for the radial axis within the first 4 s, while for the more sensitive axis X and Φ, the convergence is not yet totally finished and still in progress. Nevertheless the observation of the transient behaviour along X and Φ during the first 4 s should be sufficient to check the operability of the instrument.

Then, the simulations are exploited:

- to tune the correctors and optimise them for the test,
- to interpret the measured data by extrapolating the measured curves out of the free-fall duration to check the convergence. The simulations of the extrapolate data recorded at ZARM show that stabilization of the mass will have occurred if the duration of the fall will have allowed it.

3.1.3. Drop test sequence and precaution

Measurements of the mass position and attitude displacements with respect to the instrument structure, as well as the applied forces and torques are recorded during the test. They are available via a bi-directional RS422 link, digitalised at 1 kHz, when they transit between the ICU and the FEEU. Down link packet (FEEU to ICU) contains position sensors data and up link packet (ICU to FEEU)

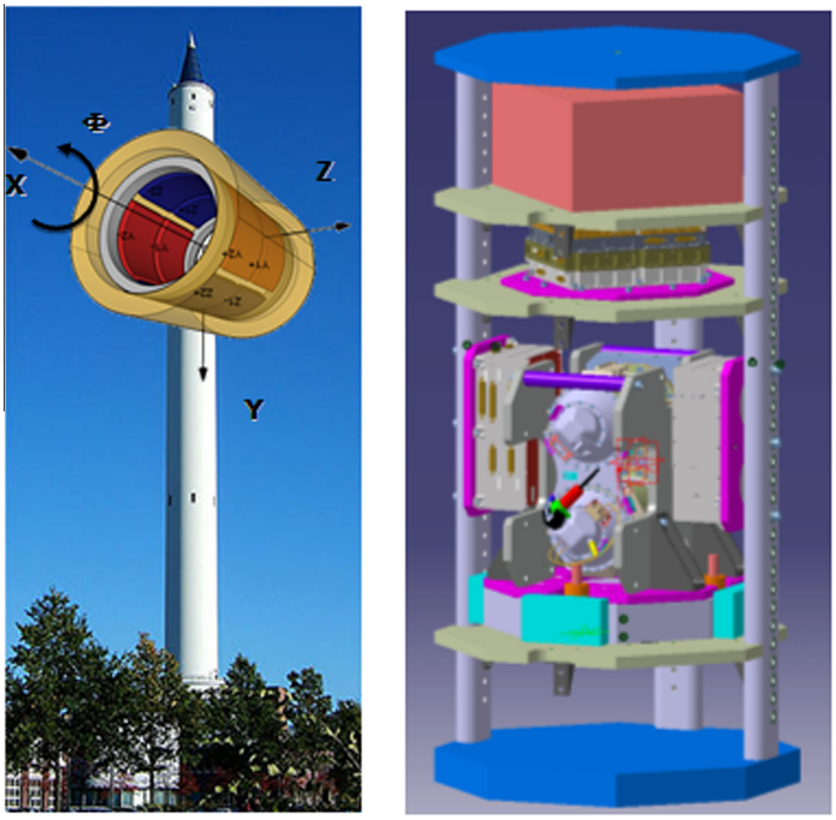

Fig. 3. *Left* – sensor core orientation during the fall. *Right* – sketch of the set up implementation in the capsule.

contains the actuation data field transmitted at 1.25 Mbaud. A spy line has been implemented to this link in order to collect all the needed data in an acquisition and storage system. The data are then buffered and dumped to a laptop after the fall.

A final pressure of about 10 Pa shall be achieved inside the drop tube in order to minimise the drag effect. When this condition is reached, just before the drop, one shall consider also the outside wind strength on the tower that introduces slight motions of the free-fall tube. The capsule pendulum motion is then monitored and the release is authorised only when a complete immobility of the capsule is obtained. A particular care is also taken to any motion part inside the capsule that may generate small vibrations which will be measured by the accelerometers: for instance, cables are carefully attached; on-board computer fans are switched-off.

3.2. Test result: control of 6 × 2 degrees of freedom of both internal and external masses

The Figs. 5–8, present a full set of measurements obtained during the 4.7 s of the fall. Fig. 5 and 6 are devoted to the internal mass and 7 and 8 to the external mass. Then, Figs. 5 and 7 show the 6 degrees of freedom (3 translations and 3 rotations) of the controlled motion of the proof masses inside the accelerometer cage as it is measured by the capacitive sensing. Figs. 6 and 8 show the corresponding measured accelerations.

Before the capsule release, under 1 g, the proof masses rely on the stops. Along the Y axis (quite vertical, direction of the fall), they rely on the lower stop at a distance of about 120 μm from the centre of the electrode set. The release of the capsule happens at 0.12 s after $t_0 = 0$ s (origin of the curve of Figs. 5–8). The end of the fall happens at $t = 4.84$ s. The duration of the fall is 4.72 s.

The instrument is switched on before the release of the capsule, so when under microgravity, the acquisition of the mass electrostatic suspension is automatically performed. As soon as the level of the capsule acceleration is within the accelerometer full range, the mass position is controlled to the centre of the set of electrodes and then the instrument measurement is de-saturated.

For the inner proof-mass, all the degrees of freedom are controlled, at the end of the fall, at the centre of the cage, except Φ attitude which necessitates a few seconds more for a complete convergence.

For the heaviest outer proof-mass, of 1.4 kg weight, the servo-loops encounter more difficulty to converge than for the inner one (weighting 0.4 kg) because it requires more forces for the same acceleration or more time to converge for the same delta of velocity.

3.3. Test result: discussion

3.3.1. Proof mass position

The proof masses at the end of the 4.72 s duration of the fall are measured at the positions given in Table 2: the

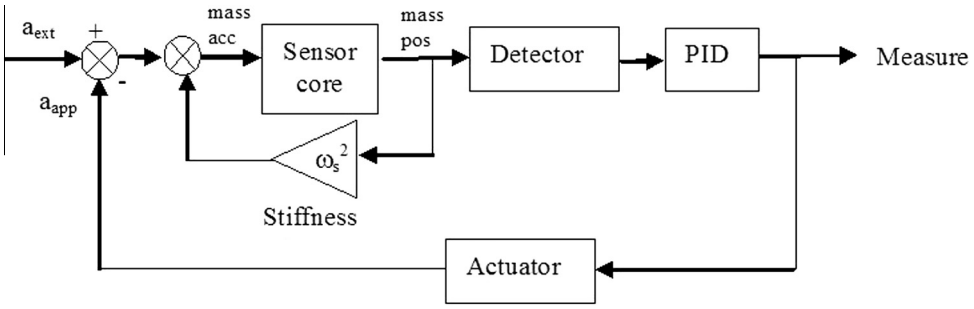

Fig. 4. Block diagram of one axis control loop.

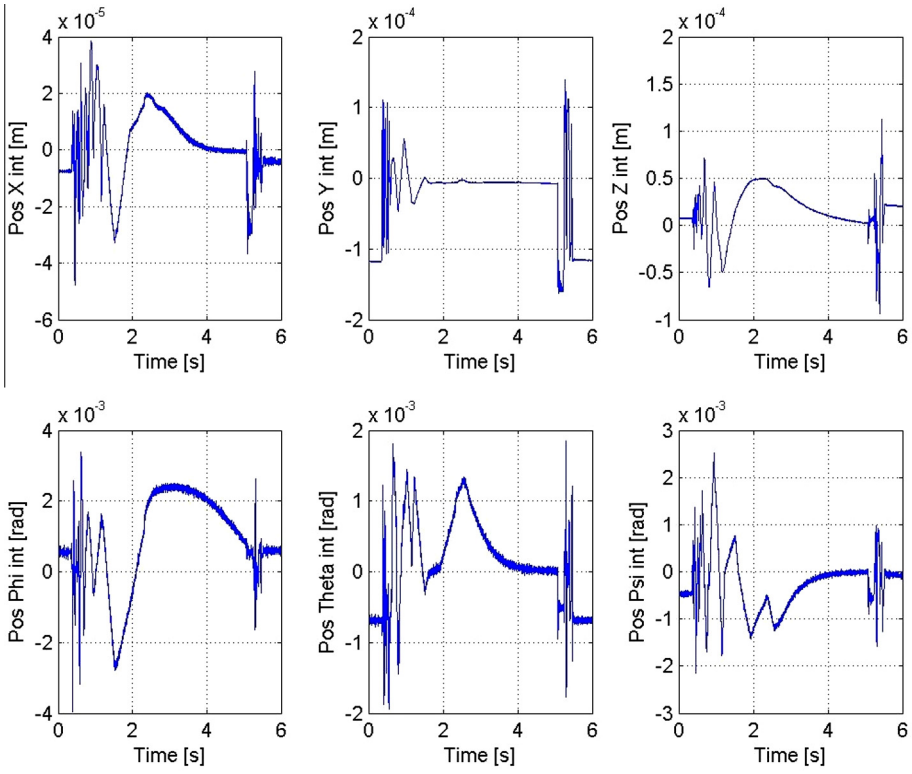

Fig. 5. Positions measured along $\{X, Y, Z, \Phi, \theta, \Psi\}$, internal test mass expressed in m or rad.

provided values are the mean measured positions over the last 0.1 s: it is interesting to filter out the vibrations at upper frequency than 5 Hz, because the servo-loops exhibit lower frequency bandwidths and theses vibrations represent the mechanical behaviour of the capsule structure after release and not the loop characteristics.

For the Y axis, the final position of about -8 μm for both masses is due to the static error of the loop in presence of the permanent residual acceleration (drag) and in absence of the integral term. This static error in position is proportional to the applied acceleration, square of the time after 3.5 s when the mass levitation is acquired.

At the same time, the accelerometer provides the acceleration of the capsule up to 195.4 μm/s^2 at t–$t_0 = 4.72$ s while the residue of the loop (in acceleration) is less than 4 μm/s^2. This measured acceleration do match with the off-centring of 8 μm with the gain loop ω_c^2 near (25 rd/s)^2.

Along the Z axis and contrarily to Y axis, the measured acceleration at the end of the fall is only 18 μm/s^2 with oscillations of ±5 μm/s^2 due to capsule elastic behaviour. By comparing Fig. 7 and 8 for this axis, we can observe that the electrostatic levitation of the mass is much acquired for the external sensor than for the internal one, leading to an important off-centring of the internal mass at the end of the fall.

The full control of both axes X is quite obtained at the end of the fall in spite of $T\text{min}_x$ much larger than $T\text{min}_{y,z}$.

3.3.2. Proof-mass attitude

The attitude θ and Ψ are controlled during the transient phase of the levitation for both test masses as expected considering Tmin (see Table 1).

For Φ attitude Tmin is of the same order of magnitude as the duration of the fall which does not allow seeing the

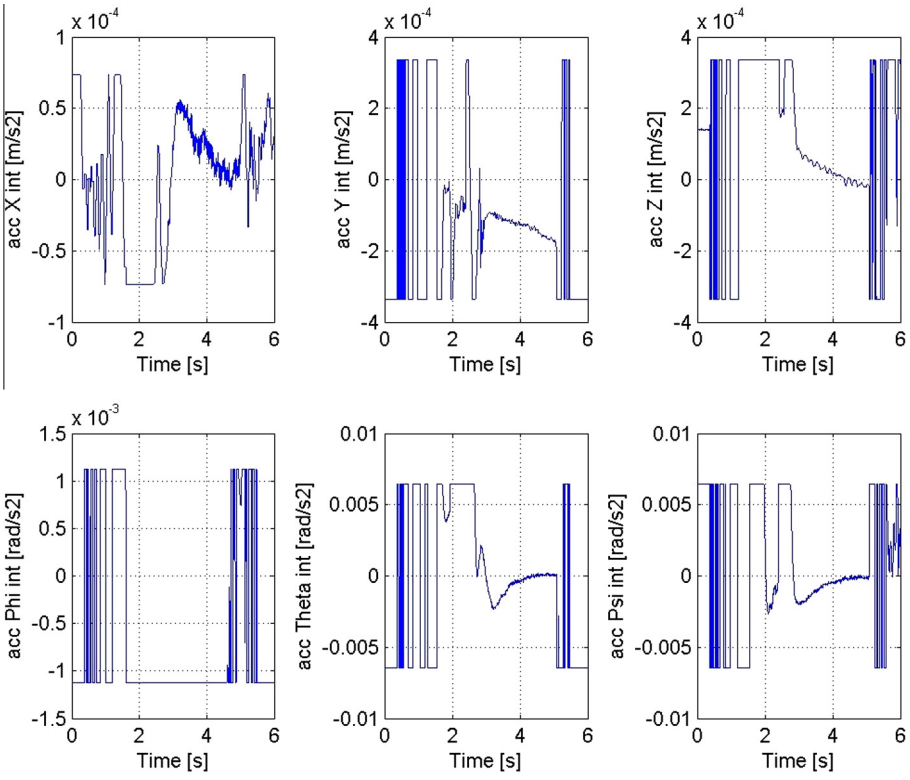

Fig. 6. Accelerations measured along $\{X, Y, Z, \Phi, \theta, \Psi\}$, internal test mass expressed in m/s^2 or rad/s^2.

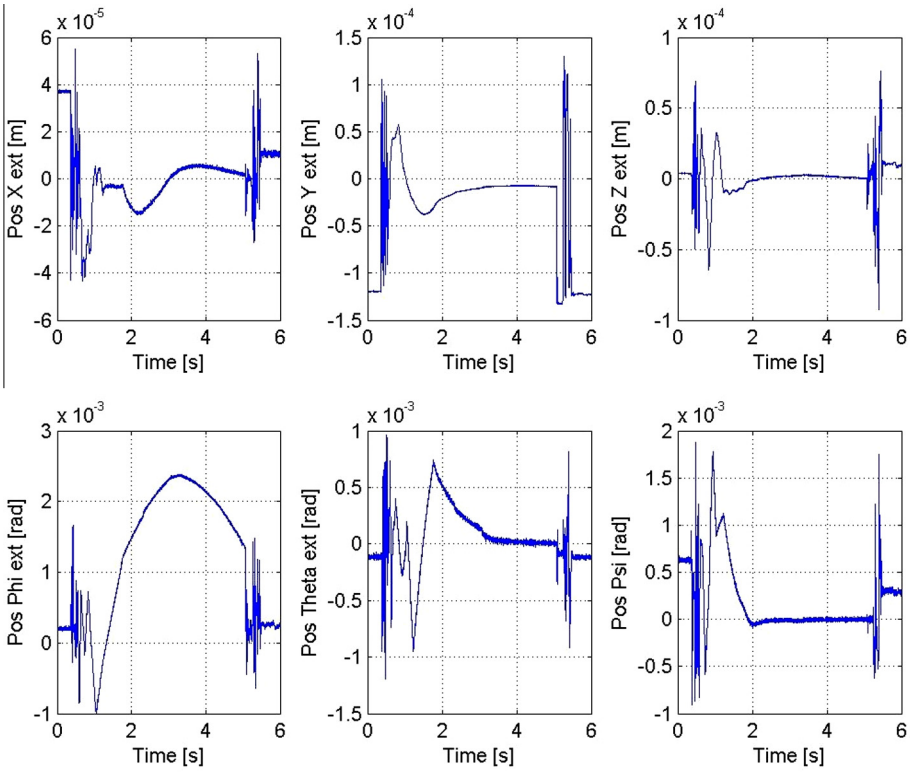

Fig. 7. Positions measured along $\{X, Y, Z, \Phi, \theta, \Psi\}$, external test mass expressed in m or rad.

end of the acquisition phase to the centre (residue of 0.83 m rad for the inner mass and 1.38 m rad for the outer mass). In this case, the Simulink simulator described in Section 3.1.2 is used to extrapolate the experimental data

Please cite this article in press as: Liorzou, F., et al. Free fall tests of the accelerometers of the MICROSCOPE mission. J. Adv. Space Res. (2014), http://dx.doi.org/10.1016/j.asr.2014.05.009

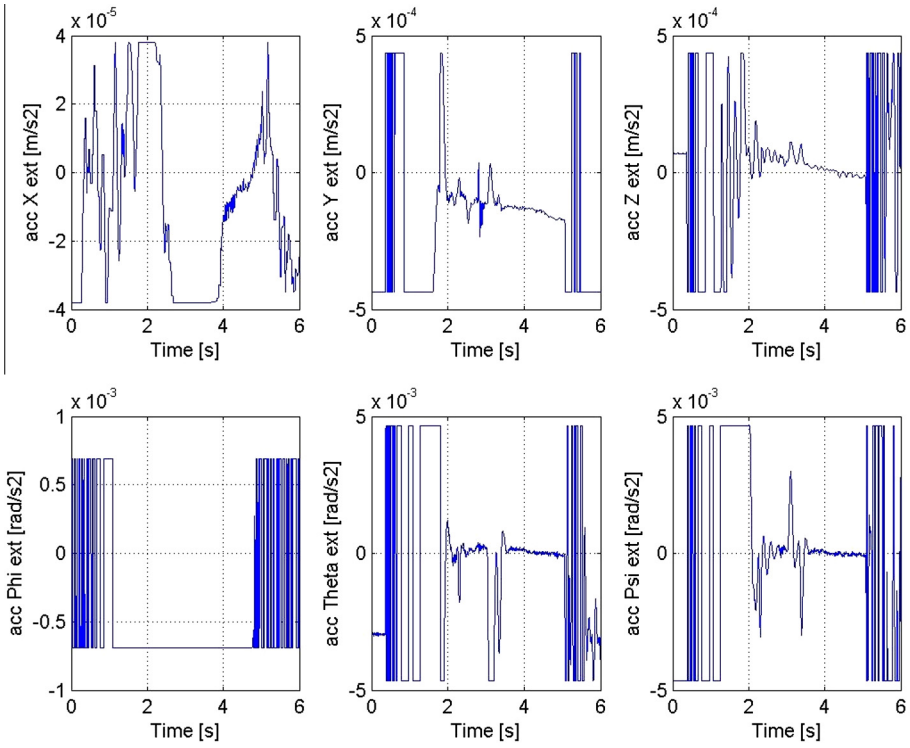

Fig. 8. Accelerations measured along $\{X, Y, Z, \Phi, \theta, \Psi\}$, external test mass expressed in m/s^2 or rad/s^2.

Table 2

Degrees of freedom	PM positions [μm] or [m rad]	
	Internal mass	External mass
X	−0.51	1.82
Y	−7.76	−8.41
Z	2.63	0.25
Φ	0.83	1.38
Θ	0.011	0.004
Ψ	−0.004	0.0004

recorded during the fall in order to obtain the final state of the control. The simulation starts at the time Ts when the test-masses are sufficiently controlled along all the other degrees of freedom: this is to avoid couplings between the other axes due to large motions of the mass or due to contacts with the mechanical stops. Ts is also chosen when the velocity of the proof-mass is null, in order to take in the simulation realistic initial conditions. Errors in the position or velocity measurements are sufficiently weak to avoid dramatic effects in the simulation. Fig. 9 shows the result obtained with the external mass Φ axis: the red curve, over the blue curve (measured data), is the result of the simulation considering the test mass position and velocity as measured at $Ts = 2.9$ s.

The simulated position of the test mass follows, from Ts to the end of the fall, the actual position and shows that the convergence is reached without oscillations after 6 s of microgravity environment.

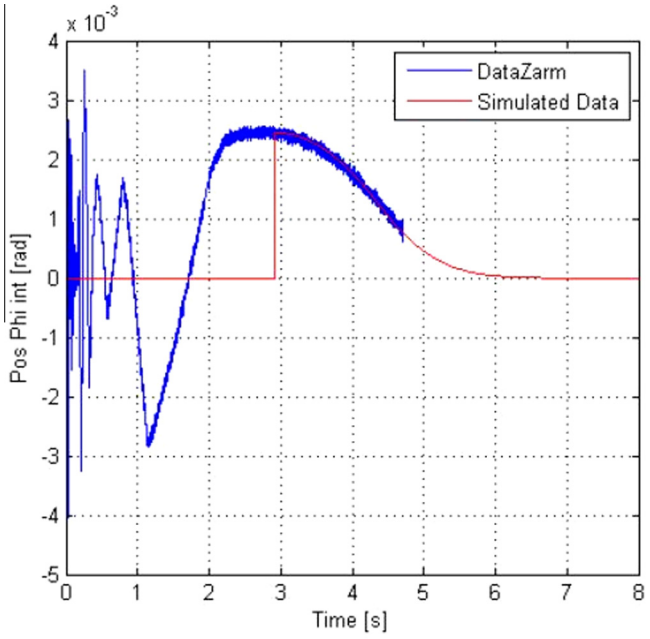

Fig. 9. Test mass position measured (blue line) and simulated (red line) along Φ axis. (For interpretation of the references to colour in this figure legend, the reader is referred to the web version of this article.)

3.3.3. First differential measures and bias estimation

The stringent short duration of a free fall leads the instrument to be configured in a coarse acquisition mode and does not allow to access to the performances expected in flight; however some characteristics can be evaluated

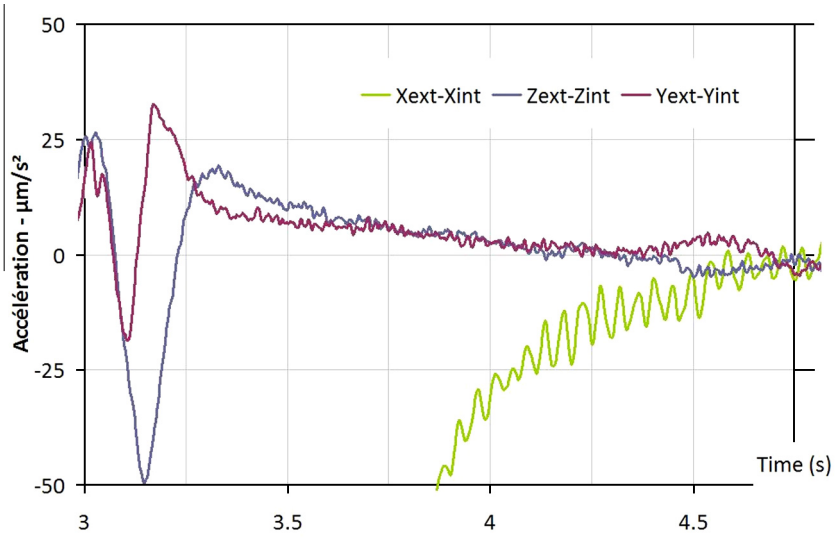

Fig. 10. Differential accelerations of X, Y and Z [µm s^{-2}].

Table 3

Degrees of freedom	Differential biases [m s^{-2}] or [rad s^{-2}]	
	Evaluations from error budget	Estimates from free falls at $t = 4.72$ s
Xext–Xint	$-8 \times 10^{-7} < \delta$ bias $< 8 \times 10^{-7}$	0.4×10^{-6}–$1.2 \times 10^{-6} = -8 \times 10^{-7}$
Yext–Yint	$-10.7 \times 10^{-5} < \delta$ bias $< 10.7 \times 10^{-5}$	$-10 \times 10^{-6} + 15 \times 10^{-6} = -5 \times 10^{-6}$
Zext–Zint	$-10.7 \times 10^{-5} < \delta$ bias $< 10.7 \times 10^{-5}$	$-10 \times 10^{-6} + 12 \times 10^{-6} = -2 \times 10^{-6}$
Θext–Θint	$-9 \times 10^{-4} < \delta$ bias $< 9 \times 10^{-4}$	9×10^{-4}–$8 \times 10^{-4} = 1 \times 10^{-4}$
Ψext–Ψint	$-9 \times 10^{-4} < \delta$ bias $< 9 \times 10^{-4}$	8.5×10^{-4}–$8 \times 10^{-4} = 5 \times 10^{-5}$

and it is interesting to analyse the differential accelerations in every direction.

The residual differential acceleration at the end of the drop due to the tangential and centrifugal acceleration of the capsule is very small because the distance between the two centres of the test masses is less than 20 µm. In fact, knowing that the angular acceleration measured by the instrument is less than 10^{-3} rad/s^2 corresponding to angular velocity of less than 10^{-3} rad/s for angular frequency higher than 1 rad/s; the corresponding difference of the linear accelerations of the two sensors are roughly evaluated respectively less than 2×10^{-8} and 2×10^{-11} m/s^2.

In addition, the Coriolis accelerations are negligible because the mass velocity after 4.7 s is less than 5 µm/s leading to 10^{-8} m/s^2 Coriolis effect.

The differential bias is deduced from the experimental data of the Fig. 10 and expressed in Table 3.

Along and about the radial axes, the position and attitude (Y, Z, θ, Ψ) of the masses being sufficiently steady and centred at the end of the drop, the measured acceleration provided by each accelerometer can be considered as the sum of the external acceleration and the accelerometer bias. Thus the simple difference of the measurements provides an estimate of the differential bias that is compared to the theoretical estimation performed for the mission (see Table 3).

Bias along Φ is not mentioned because not properly measured since the transient phase is much longer than the duration of the fall.

The deduced estimated biases from the drop data are in good agreement with the error budget (see Table 3).

3.3.4. Scale factor estimation

The scale factor of the instrument is estimated through the geometrical and the electrical parameters of the sensor: for the internal accelerometer Y axis, it is estimated to 241 µm/s^2/V while for the external it is estimated to 310 µm/s^2/V leading to a ratio of 1.286.

Along the fall axis, acceleration due to the atmospheric drag is systematically observed because of the residual pressure within the tube of (10–15 Pa at capsule release). This provides a non null signal measured by both, the inner and the outer acceleration sensors. It is a function of time^2 and both measurements can be fitted by polynomial functions that are compared. Therefore as a first approach illustrated in Fig. 11, the ratio between the polynomial coefficients gives a rough estimate about the scale factor matching. This leads to 5.7% with the quadratic coefficient and 3.7% with the linear. However, this approach is penalised by the residual oscillations of the processed signals (fits are obtained with a normalised residue $\sigma^2 = 8 \times 10^{-2}$).

Please cite this article in press as: Liorzou, F., et al. Free fall tests of the accelerometers of the MICROSCOPE mission. J. Adv. Space Res. (2014), http://dx.doi.org/10.1016/j.asr.2014.05.009

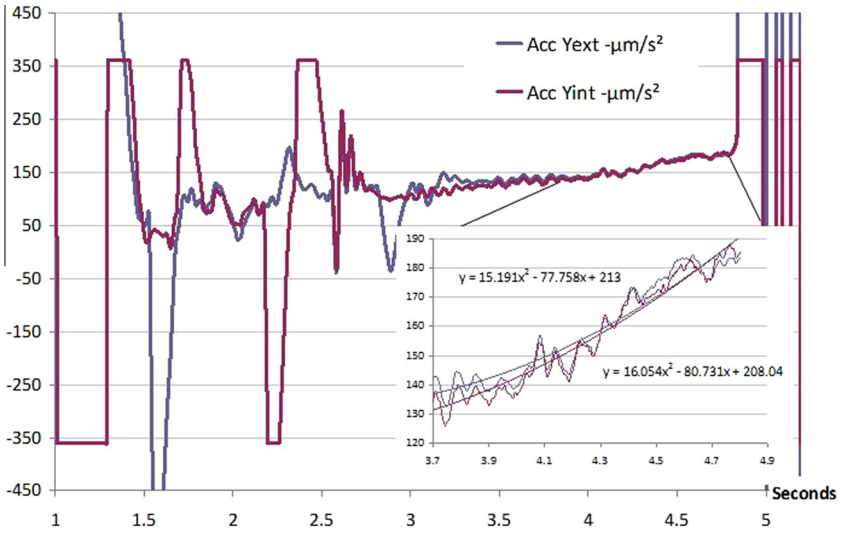

Fig. 11. Example of extrapolated data and polynomial fit of the residual atmospheric drag acceleration along *Y*-axis (both test-masses).

A more accurate method consists in applying a mean square estimation of the ratio of the un-scale experimental data of both test masses and compares it to the "as design" ratio (1.286). It leads to a matching of 1.2% ($\sigma = 0.5\%$. It can be compared with the GOCE legacy. During the on ground test dedicated to this mission, such error were evaluated to 0.3% about, keeping in mind that for GOCE accelerometers, it was possible to levitate the proof-masses under 1 g and then test extensively during hours the horizontal axes.

4. Conclusion

The acquisition and the control of the electrostatic levitation (6 degrees of freedom) of the two cylindrical proof masses of the MICROSCOPE instrument have been successfully tested for the first time in the BREMEN drop tower. This success is an important step for the development of the MICROSCOPE mission. It contributes to the qualification of the instrument by confirming the good operation of the twelve electrostatic digital loops in micro gravity and the good reliability and robustness of the configuration. Five campaigns, with a total of 45 falls, have been conducted so far in order to provide a better assessment of the dynamical behaviour of the instrument.

Thanks to these experiments, a typical dynamical response, with optimised control laws vs. controller's bandwidth and fall duration, has been defined. This allows the establishment of qualification and acceptance criteria for the MICROSCOPE flight models.

Acknowledgement

The authors want to acknowledge the CNES for their support and funding to develop the payload, the ZARM for their contribution to the qualification and acceptance tests of the payload in free fall conditions. Part of the work is funded by ONERA.

References

Touboul, P., Métris, G., Lebat, V., Robert, A., 2012a. The MICROSCOPE experiment, ready for the in orbit test of the Equivalence Principle. Classical Quantum Gravity 29, 184010.

Hudson, D., Chhun, R., Touboul, P., 2007. Development status of the differential accelerometer for the MICROSCOPE mission. Adv. Space Res. 39 (2), 307–314. http://dx.doi.org/10.1016/j.asr.2005.10.040.

Touboul, P., Foulon, B., Christophe, B., Marque, J.P., 2012b. CHAMP, GRACE, GOCE instruments and beyond, geodesy for planet earth. In: Kenyon, S., et al. (Eds.), IAGS, vol. 136, pp. 215–221.

Christian Eigenbrod and the Drop Tower Operation and Service Company, 2007. ZARM Drop Tower Bremen User Manual, 41, ZARM FABmbh, Bremen.

Guiu, E., Rodrigues, M., Touboul, P., et al., 2007. Calibration of MICROSCOPE. Adv. Space Res. 39 (2), 315–323. http://dx.doi.org/10.1016/j.asr.2006.06.012.

Touboul, P., 2009. The MICROSCOPE mission and its uncertainty analysis. Space Sci. Rev., 148455–148474.